

Silicon mode (de)multiplexers with parameters optimized using shortcuts to adiabaticity

DEFEN GUO^{1,3} AND TAO CHU^{1,2,*}

¹*Institute of Semiconductors, Chinese Academy of Sciences, P.O. Box 912, Beijing 100083, China*

²*College of Information Science and Electronic Engineering, Zhejiang University, 38 Zheda Road, Hangzhou 310027, China*

³*University of Chinese Academy of Sciences, 19 A Yuquan Rd, Shijingshan District, Beijing 100049, China*

*chutao@zju.edu.cn

Abstract: We propose and experimentally demonstrate broadband silicon mode (de)multiplexers based on the optimization of system adiabaticity using shortcuts to adiabaticity (STA). The measured insertion losses and crosstalks were less than 1.1 dB and -24 dB, respectively, for the five two-mode mode-division-multiplexing (MDM) links over wavelengths ranging from 1500 nm to 1600 nm. The four-mode MDM link showed measured insertion losses and crosstalks less than 1.3 dB and -23 dB, respectively, within the same wavelength range. The method paves the way for future adaptation of the STA protocols to various components.

© 2017 Optical Society of America

OCIS codes: (060.1810) Buffers, couplers, routers, switches, and multiplexers; (060.4230) Multiplexing; (130.3120) Integrated optics devices; (230.7370) Waveguides.

References and links

1. P. Dong, "Silicon Photonic Integrated Circuits for Wavelength-Division Multiplexing Applications," *IEEE J. Sel. Top. Quantum Electron.* **22**(6), 370–378 (2016).
2. T. Ye, Y. Fu, L. Qiao, and T. Chu, "Low-crosstalk Si arrayed waveguide grating with parabolic tapers," *Opt. Express* **22**(26), 31899–31906 (2014).
3. L.-W. Luo, N. Ophir, C. P. Chen, L. H. Gabrielli, C. B. Poitras, K. Bergmen, and M. Lipson, "WDM-compatible mode-division multiplexing on a silicon chip," *Nat. Commun.* **5**, 3069 (2014).
4. D. Dai, J. Wang, and Y. Shi, "Silicon mode (de)multiplexer enabling high capacity photonic networks-on-chip with a single-wavelength-carrier light," *Opt. Lett.* **38**(9), 1422–1424 (2013).
5. Y. Kawaguchi and K. Tsutsumi, "Mode multiplexing and demultiplexing devices using multimode interference couplers," *Electron. Lett.* **38**(25), 1701–1702 (2002).
6. M. Ye, Y. Yu, J. Zou, W. Yang, and X. Zhang, "On-chip multiplexing conversion between wavelength division multiplexing-polarization division multiplexing and wavelength division multiplexing-mode division multiplexing," *Opt. Lett.* **39**(4), 758–761 (2014).
7. C. Pan and B. M. A. Rahman, "Accurate Analysis of the Mode (de)multiplexer Using Asymmetric Directional Coupler," *J. Lightwave Technol.* **34**(9), 2288–2296 (2016).
8. J. B. Driscoll, R. R. Grote, B. Souhan, J. I. Dadap, M. Lu, and R. M. Osgood, "Asymmetric Y junctions in silicon waveguides for on-chip mode-division multiplexing," *Opt. Lett.* **38**(11), 1854–1856 (2013).
9. W. Chen, P. Wang, T. Yang, G. Wang, T. Dai, Y. Zhang, L. Zhou, X. Jiang, and J. Yang, "Silicon three-mode (de)multiplexer based on cascaded asymmetric Y junctions," *Opt. Lett.* **41**(12), 2851–2854 (2016).
10. J. Xing, Z. Li, X. Xiao, J. Yu, and Y. Yu, "Two-mode multiplexer and demultiplexer based on adiabatic couplers," *Opt. Lett.* **38**(17), 3468–3470 (2013).
11. J. Wang, Y. Xuan, M. Qi, H. Huang, Y. Li, M. Li, X. Chen, Z. Sheng, A. Wu, W. Li, X. Wang, S. Zou, and F. Gan, "Broadband and fabrication-tolerant on-chip scalable mode-division multiplexing based on mode-evolution counter-tapered couplers," *Opt. Lett.* **40**(9), 1956–1959 (2015).
12. L. F. Frellsen, Y. Ding, O. Sigmund, and L. H. Frandsen, "Topology optimized mode multiplexing in silicon-on-insulator photonic wire waveguides," *Opt. Express* **24**(15), 16866–16873 (2016).
13. S. Martínez-Garaot, S.-Y. Tseng, and J. G. Muga, "Compact and high conversion efficiency mode-sorting asymmetric Y junction using shortcuts to adiabaticity," *Opt. Lett.* **39**(8), 2306–2309 (2014).
14. S.-Y. Tseng, R.-D. Wen, Y.-F. Chiu, and X. Chen, "Short and robust directional couplers designed by shortcuts to adiabaticity," *Opt. Express* **22**(16), 18849–18859 (2014).
15. T.-H. Pan and S.-Y. Tseng, "Short and robust silicon mode (de)multiplexers using shortcuts to adiabaticity," *Opt. Express* **23**(8), 10405–10412 (2015).

16. C.-P. Ho and S.-Y. Tseng, "Optimization of adiabaticity in coupled-waveguide devices using shortcuts to adiabaticity," *Opt. Lett.* **40**(21), 4831–4834 (2015).
17. M. L. Cooper and S. Mookherjea, "Numerically-assisted coupled-mode theory for silicon waveguide couplers and arrayed waveguides," *Opt. Express* **17**(3), 1583–1599 (2009).

1. Introduction

Many researchers consider silicon photonic integration to be one of the most promising techniques for realizing high-density and high-speed optical interconnects because it offers compact device size and complementary metal-oxide-semiconductor (CMOS)-compatible fabrication processes. Along with traditional wavelength-division-multiplexing (WDM) technology [1,2], mode-division-multiplexing (MDM) has attracted much recent attention for adding a new physical dimension to keep pace with the increasing capacity requirements of high-performance computers and data centers [3]. A high-performance mode (de)multiplexer with low insertion loss, low crosstalk, broad bandwidth, and large fabrication tolerance is the key component for achieving MDM. Two schemes are generally used to design mode (de)multiplexers. One, based on mode interference, includes asymmetrical directional couplers (ADC) [3,4] and multimode interferometer couplers (MMI) [5,6]. The performance of ADC-based (de)multiplexers is sensitive to wavelength, coupling length, and waveguide width [7]. MMI-based (de)multiplexers are not easy to extend to higher-order modes. The second approach, based on the adiabatic scheme, includes asymmetrical Y junctions [8,9] and adiabatic couplers [10,11]. It is difficult for the asymmetrical Y junctions to achieve low-loss corners in fabrication and the lengths of the adiabatic couplers need to be sufficient to maintain the slow evolution of local modes. Topology-optimized-based (de)multiplexers have been reported recently, but the crosstalk they exhibit is relatively high, and their fabrication precision is strictly required [12].

Recently, the protocols of shortcuts to adiabaticity (STA) have been proposed as conceptual guides for developing designs of different types of photonic devices to shorten the lengths of adiabatic couplers [13–16]. Short and robust mode (de)multiplexers have been designed by combining the STA protocol and perturbation theory [15]. However, the (de)multiplexers, which belong to the Δ -coupler [14], are only optimized to the possible errors arising from the propagation-constant mismatch. The possible errors of the coupling coefficient are not optimized. A design that is insensitive to the errors of propagation-constant mismatch may be sensitive to the errors of the coupling coefficient [16]. In addition, the bent multimode waveguide for the structure in [15] may introduce significant mode crosstalk when cascading (de)multiplexers of different orders.

In this letter, we experimentally demonstrated STA-based high-performance mode (de)multiplexers for the first time. Instead of using the Δ -coupler based (de)multiplexers [15], we optimized the adiabaticity of (de)multiplexers by designing the system evolution to be as close to the adiabatic state as possible [16]. The (de)multiplexers had straight bus waveguides, which is appropriate for use in cascades. Results for all transverse electric (TE) modes showed that the simulated TE0-to-TE1, TE0-to-TE2, and TE0-to-TE3 (hereafter, TE i –TE j) conversion losses were less than 0.3 dB and the mode crosstalks were lower than –40 dB over a wide wavelength range from 1450 nm to 1650 nm. Results for all transverse magnetic (TM) modes indicated that the simulated TM0–TM1 and TM0–TM2 conversion losses were less than 0.7 dB and the mode crosstalks were lower than –30 dB within the same wavelength range. With fabricated MDM links consisting of combined mode multiplexers and demultiplexers together, the experimental results showed that the insertion losses of all MDM links were less than 1.3 dB and the mode crosstalks were lower than –23 dB over the measured wavelengths ranging from 1500 nm to 1600 nm.

2. Coupler design and simulation

As shown in Fig. 1(a), the STA-based mode (de)multiplexer consists of a single-mode access waveguide and a multimode bus waveguide. The width of the multimode bus waveguide is set, in each configuration, to a fixed value W_b . The width of the single-mode access waveguide $W_a(z)$ and the separation $D(z)$ between the access and bus waveguides change continuously with the propagation direction z . A_0 is set as the amplitude of the fundamental mode in the access waveguide, and A_m is set as the amplitude of the m th mode in the bus waveguide. Then, the changes of the guided-mode amplitude in the individual waveguides $|\Psi\rangle = [A_0, A_m]^T$ with the propagation distance can be described by the coupled-mode equation

$$\frac{d}{dz} \begin{bmatrix} A_0 \\ A_m \end{bmatrix} = -i \begin{bmatrix} -\Delta(z) & K(z) \\ K(z) & \Delta(z) \end{bmatrix} \begin{bmatrix} A_0 \\ A_m \end{bmatrix}, \quad (1)$$

where $K(z)$ denotes the coupling coefficient, and $\Delta(z)$ denotes the propagation-constant mismatch.

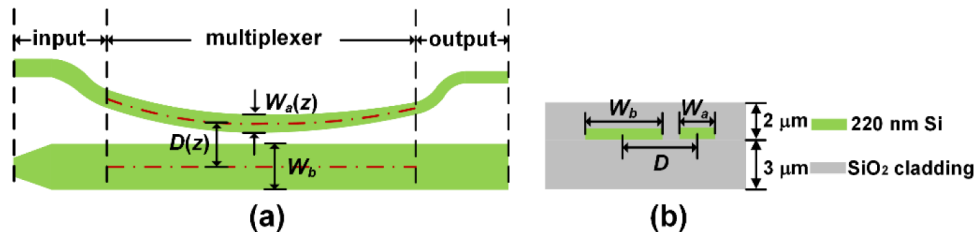


Fig. 1. Schematic diagrams of the optimized mode (de)multiplexer using STA. (a) Top view. (b) Side view.

The initial and final states of the system can be set to $|\Psi(0)\rangle = [0, 1]^T$ and $|\Psi(L)\rangle = [1, 0]^T$, respectively. Using the invariant-based STA approach, the solution of Eq. (1) can be described by the states [14]

$$|\Psi_z^+\rangle = \cos(\theta/2) e^{-i\phi/2} |\Psi(L)\rangle + \sin(\theta/2) e^{i\phi/2} |\Psi(0)\rangle \quad (2)$$

and

$$|\Psi_z^-\rangle = \sin(\theta/2) e^{-i\phi/2} |\Psi(L)\rangle - \cos(\theta/2) e^{i\phi/2} |\Psi(0)\rangle, \quad (3)$$

where

$$d\theta/dz = K \sin \phi \quad (4)$$

and

$$d\phi/dz = \Delta + K \cos \phi \cot \theta \quad (5)$$

Considering the boundary conditions and completing some mathematical derivations leads to expressions for the smooth functions of θ and ϕ [16], namely

$$\theta = \frac{\pi}{2} \left[1 + \sin \frac{\pi(2z-L)}{2L} \right] \quad (6)$$

and

$$\begin{aligned}\phi(z) = & \frac{\pi}{2} + \left(\frac{\pi}{2} - c\right) \cdot (-1.1250) \sin\left(\frac{\pi z}{L}\right) \\ & + \left(\frac{\pi}{2} - c\right) \cdot (-0.1250) \sin\left(\frac{3\pi z}{L}\right),\end{aligned}\quad (7)$$

where c is a parameter related to the maximum derivative of θ and maximum coupling coefficient K_{max} of the coupled-mode system and can be calculated using $c = \arcsin((d\theta/dz)_{max}/K_{max})$. Here, the third-order Fourier expansion of φ is adopted. Equations (4), (5), (6), and (7) can be used to derive the optimized values of the coupling coefficient $K(z)$ and the propagation-constant mismatch $\Delta(z)$ with the propagation direction. Then, the relation between the coupling coefficient $K(z)$ and waveguide separation $D(z)$ can be fitted by the exponential relation

$$K(z) = K_0 \exp[-k(D(z) - D_0)], \quad (8)$$

where K_0 , k , and D_0 are the fitting coefficients. Next, the relation between the propagation-constant mismatch $\Delta(z)$ and the waveguide width $W_a(z)$ can be approximated by the polynomial relation

$$\Delta(z) = A * W_a(z)^2 + B * W_a(z) + C, \quad (9)$$

where A , B , and C are the fitting coefficients.

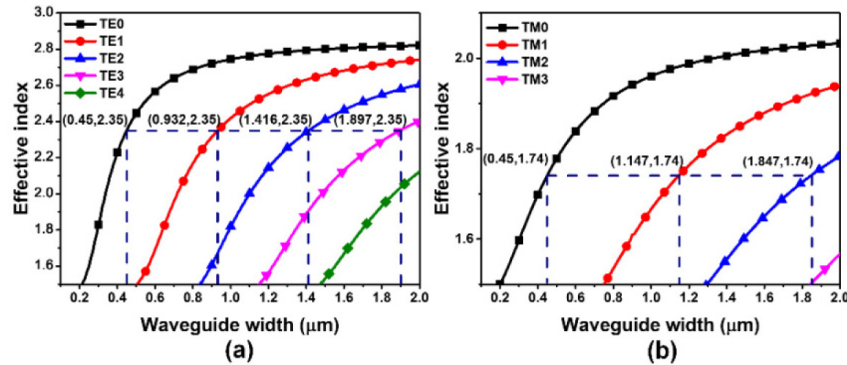


Fig. 2. Calculated effective indices for different TE and TM modes in a 220-nm-high strip waveguide versus different waveguide widths at 1550 nm. (a) TE modes. (b) TM modes.

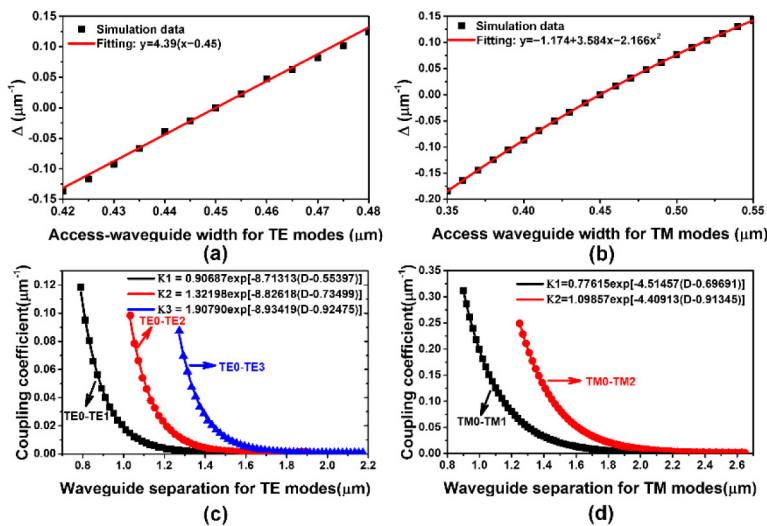


Fig. 3. Relations between propagation-constants mismatch and access-waveguide widths and between coupling coefficients and waveguide separations. (a) and (c) TE modes. (b) and (d) TM modes.

As Fig. 1(b) shows, the mode (de)multiplexers were designed on a silicon-on-insulator (SOI) wafer. The silicon core thickness was 220 nm. The thicknesses of the SiO_2 cladding above and below were 2 μm and 3 μm , respectively. First, the effective indices for different waveguide widths were calculated using a finite element method. The initial width of the single-mode access waveguide was chosen to be 450 nm. As Fig. 2 shows, the phase-matching widths of the bus waveguide for the TE1, TE2, and TE3 modes were 932 nm, 1416 nm, and 1897 nm, respectively. The phase-matching widths for the TM1 and TM2 modes were 1147 nm and 1847 nm, respectively. Then, the propagation-constant mismatch was calculated around the width of 450 nm and fitted by the polynomial function, as shown in Figs. 3(a) and 3(b). The linear relation is used for the TE-mode devices and quadratic relation is used for the TM-mode devices. In a small variation range, the data can be fitted well by the linear relation. However, it is more accurate to use the quadratic relation for a relatively larger range. The coupling coefficient was calculated for the phase-matching widths and fitted by the exponential function, as shown in Figs. 3(c) and 3(d).

Minimum widths of 160 nm (for TE modes) and 200 nm (for TM modes) for the edge-gaps between the access and bus waveguides were chosen after considering the fabrication conditions and device length. A shorter coupler length may require a smaller minimum edge-gap to satisfy the equations above while a longer coupler length reduces the component density. In this study, we chose lengths of 150 μm and 100 μm for the TE and TM modes, respectively. The values of the width, coupling length, minimum edge-gap, maximum coupling coefficient, and c for each mode (de)multiplexer are listed in Table 1.

Table 1. Values of the parameters for each mode (de)multiplexer

	Initial W_a (μm)	W_b (μm)	Coupling length (μm)	Minimum edge-gap (μm)	K_{max} μm^{-1}	c
TE0-TE1	0.45	0.932	150	0.16	0.06589	0.5228
TE0-TE2	0.45	1.416	150	0.16	0.05408	0.6540
TE0-TE3	0.45	1.897	150	0.16	0.04755	0.7641
TM0-TM1	0.45	1.147	100	0.2	0.1995	0.25
TM0-TM2	0.45	1.847	100	0.2	0.1622	0.3092

The relations, equations, and values described above were used to calculate the corresponding design parameters of the mode (de)multiplexers, as shown in Fig. 4. The range of the access-waveguide width variations is within 0.42–0.48 μm and 0.35–0.55 μm for the TE-mode and TM-mode (de)multiplexers, respectively. The width variations relate to the coupling coefficients and coupling lengths. The larger the coupling coefficient, the larger are the width variations of the access waveguide. The longer the coupling length, the smaller are the width variations of the access waveguide. The coupling coefficients are larger and the coupling lengths are smaller for the TM-mode (de)multiplexers than for the TE-mode (de)multiplexers. The waveguide separations have large variations in both the TE-mode and TM-mode (de)multiplexers. The waveguide separation underwent rapid changes at the beginning and end of the couplers, where the coupling coefficients are close to 0. These rapid changes correspond to large waveguide bends. The simulation and fabrication processes must eliminate these parts to reduce the insertion loss. Taking the TE0-TE1 (de)multiplexers as an example, we eliminated the parts where the edge-gaps are larger than 0.65 μm .

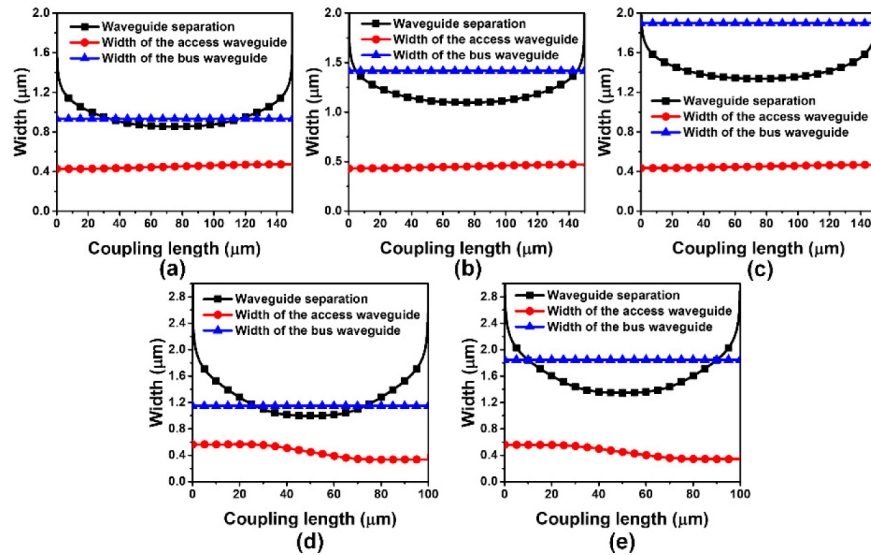


Fig. 4. Calculated design parameters of the mode (de)multiplexers. (a) TE0 and TE1. (b) TE0 and TE2. (c) TE0 and TE3. (d) TM0 and TM1. (e) TM0 and TM2.

The couplers with the derived design parameters were simulated with commercial software employing the finite-difference time-domain (FDTD) method (FDTD Solutions, Lumerical Solutions, Inc., Vancouver, Canada). Figure 5 shows the simulation results. The conversion losses incurred in moving from the input to the desired output modes were all less than 0.7 dB over wavelengths ranging widely from 1450 nm to 1650 nm. The inset pictures in Fig. 5 show the power distributions from the input mode to the output TE1, TE2, TE3, TM0, and TM1 modes, respectively, at 1550 nm. These illustrations show clearly that the input mode of the access waveguide turned into the desired modes in the bus waveguide. In addition, the mode crosstalks of the input mode to the output undesired modes were all lower than -30 dB within the same wavelength range.

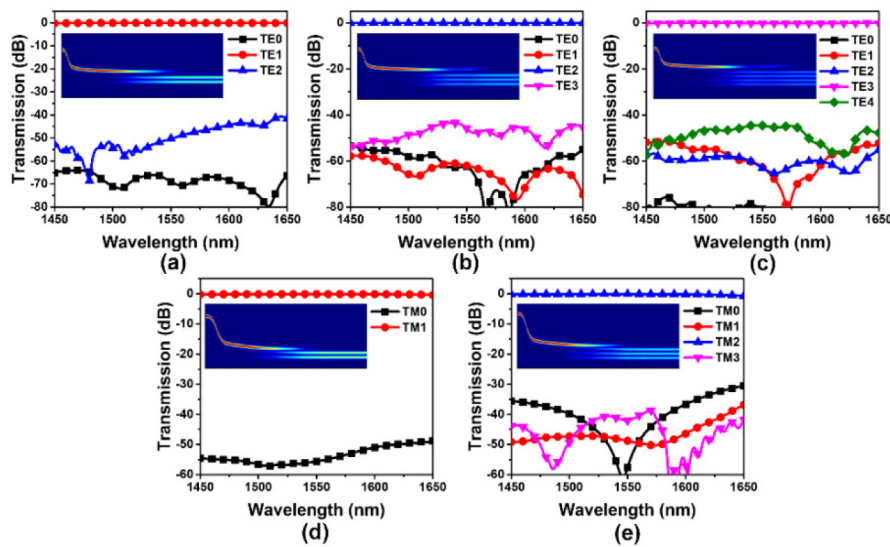


Fig. 5. FDTD simulation results of the mode (de)multiplexers. (a) TE0 and TE1. (b) TE0 and TE2. (c) TE0 and TE3. (d) TM0 and TM1. (e) TM0 and TM1. The inset pictures display the power distributions from the input mode to the desired output modes at 1550 nm.

3. Fabrication, measurements, and discussion

3.1 Fabrication and characterization method

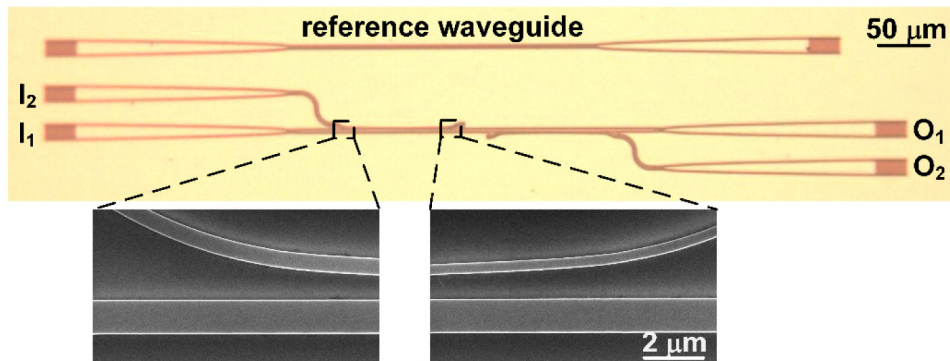


Fig. 6. Microscopic and partial scanning electron microscope (SEM) images of the fabricated TM0-TM1 MDM link.

A series of mode (de)multiplexers were fabricated and measured to obtain experimental validation of the characteristics of the optimized couplers. Processes involving electron-beam lithography (EBL), inductively coupled plasma (ICP), and plasma-enhanced chemical-vapor deposition (PECVD) were used to fabricate the devices. The mode multiplexers and demultiplexers were combined with a straight multimode waveguide between them to form the MDM links. Figure 6 shows the microscopic and partial SEM images of the TM0-TM1 MDM link. The SEM images illustrate the use of smoothly curved waveguides at the input and output parts of the mode multiplexer. The measurements of the MDM links were conducted with systems comprising a tunable laser (Santec TLS-510c), a polarization controller, fiber alignment stages (Suruga ES3700 with 50 nm alignment resolution), an optical spectrum analyzer (Yokogawa AQ6370c), and an optical power meter (Yokogawa

AQ2200-221). A pair of uniform grating couplers was used to receive/transmit the light from/into single-mode fibers.

3.2 Two-mode MDM links

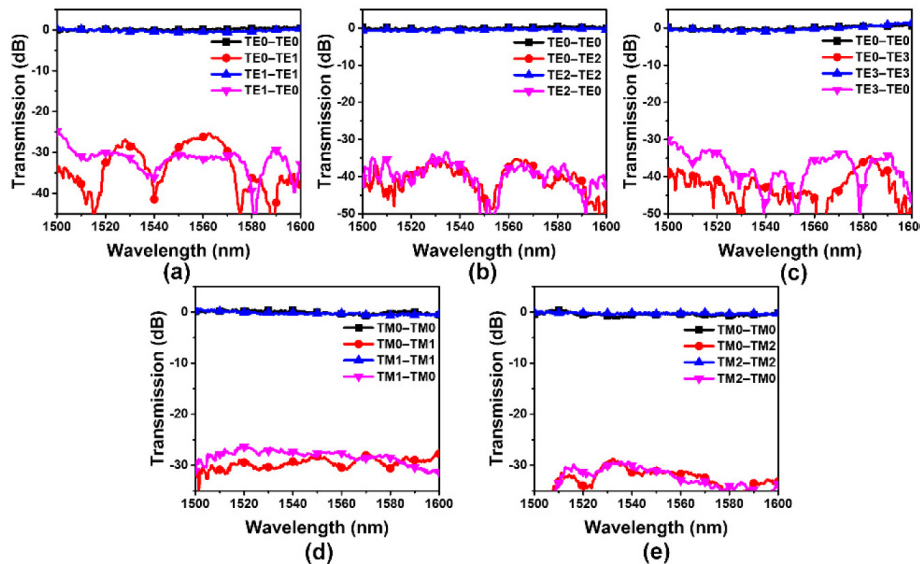


Fig. 7. Experimental results of the two-mode MDM links. (a) TE0 and TE1. (b) TE0 and TE2. (c) TE0 and TE3. (d) TM0 and TM1. (e) TM0 and TM2.

Figures 7(a)–7(e) show the normalized transmission spectra responses of the TE0–TE1, TE0–TE2, TE0–TE3, TM0–TM1, and TM0–TM2 MDM links, respectively. The transmission spectra were recorded for wavelengths ranging from 1500 nm to 1600 nm and were normalized to the spectrum of straight reference waveguides. It can be seen from the figures that insertion losses displayed no obvious degradation over the entire measured wavelength range. The maximum losses of TE0–TE i –TE0 ($i = 0, 1, 2, 3$) and TM0–TM i –TM0 ($i = 0, 1, 2$) were 1.1 dB, and the maximum crosstalks to undesired modes were –24 dB. The measured losses were slightly higher than the simulated losses, resulting mainly from the fabrication process. The insertion losses could be improved by optimizing the fabrication process. The demonstrated broadband operation was limited by the available bandwidth of the grating couplers.

3.3 Four-mode MDM link

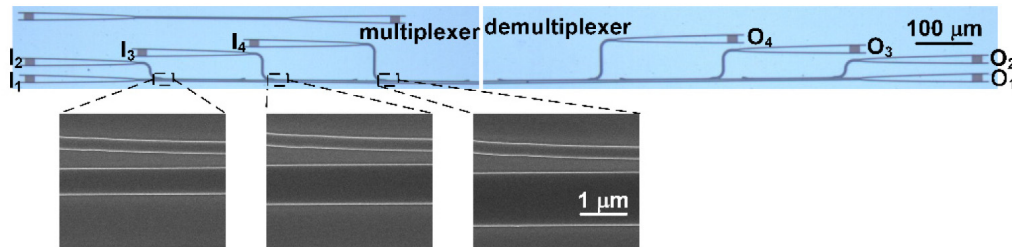


Fig. 8. Microscopic and partial SEM pictures of the fabricated four-mode (de)multiplexer with optimized parameters.

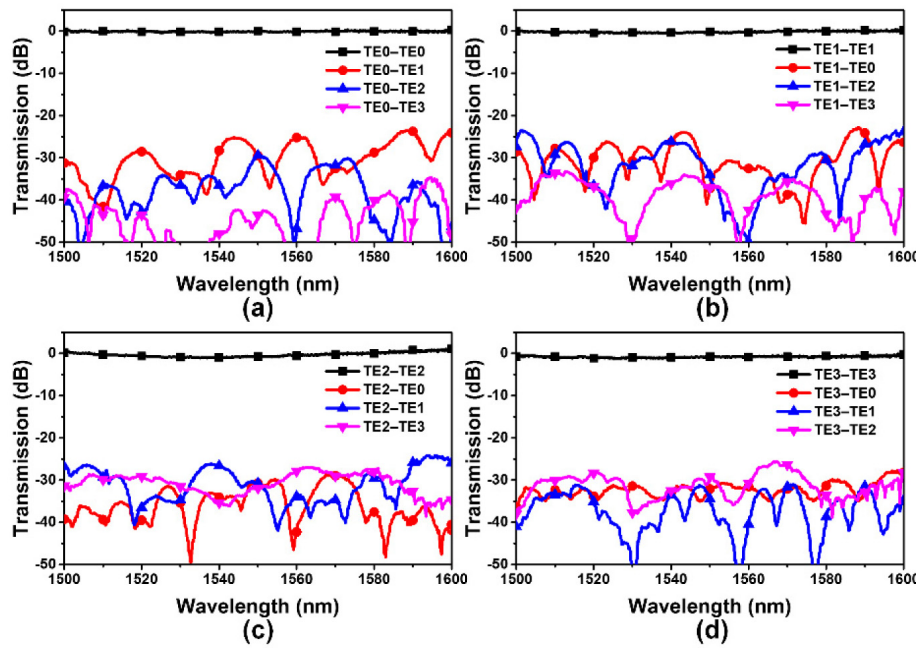


Fig. 9. Measured spectra responses of the fabricated four-mode MDM link at all output ports.

A four-mode MDM link for TE modes was fabricated and used to validate the scalability of the STA-based mode multiplexers, as Fig. 8 shows. Figures 9(a)–9(d) show the normalized transmission spectra responses for channels TE0, TE1, TE2, and TE3, respectively. The figures indicate that the light was output dominantly from the corresponding output ports. The losses of the TE0 channel were slightly lower than the losses for channels TE1, TE2, and TE3 because the higher-order modes channels required two mode conversion while the TE0 channel performed like a straight waveguide without any mode conversion. The maximum insertion loss of TE0–TE i –TE0 ($i = 0, 1, 2, 3$) was 1.3 dB over the entire range of measured wavelengths from 1500 nm to 1600 nm. The maximum crosstalk to undesired modes was –23 dB. The performance of the four-mode MDM link for the same channel showed little degradation in comparison to the measured results of the two-mode MDM links reported above.

3.4 Discussion

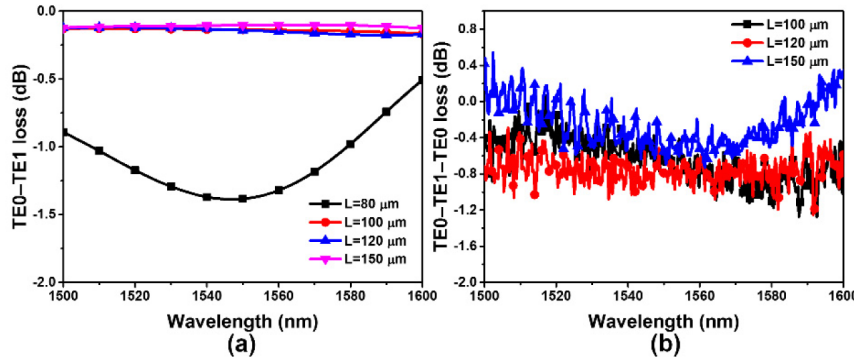


Fig. 10. Losses experienced by the TE0–TE1 (de)multiplexer. (a) Simulated insertion. (b) Measured insertion.

The tested four-mode (de)multiplexer had a minimum waveguide edge gap of 160 nm and a coupling length of 150 μm . The device length could be reduced further. Figures 10(a) and 10(b), presenting examples using the TE0–TE1 mode (de)multiplexer, show simulated and measured insertion losses at different coupling lengths, respectively. The performance of the MDM link displayed no obvious deterioration when the coupling length was reduced to 100 μm . The measured maximum insertion loss of TE0–TE1–TE0 remained less than 1.3 dB. The corresponding minimum coupling length required to satisfy the equations of STA is approximately 80 μm . However, from Fig. 10(a), we can see that the performance of $L = 80 \mu\text{m}$ (de)multiplexer degrades significantly. This may be attributed to the fact that the simple coupled-mode equation in Eq. (1) is valid under the scalar and paraxial approximation and under the assumption of weak coupling, and can only approximately apply to the high index-contrast SOI waveguides [17].

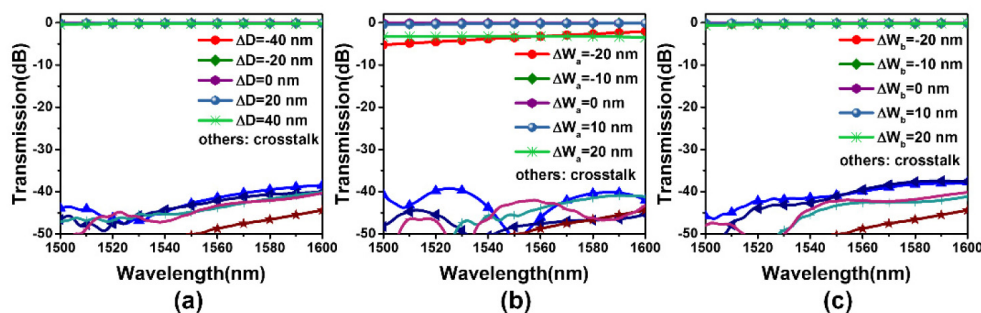


Fig. 11. Simulated TE0–TE1 conversion efficiencies for the possible fabrication errors of (a) waveguide separation, (b) width of the access waveguide, and (c) width of the bus waveguide, when the coupling length is 150 μm .

Figure 11 depicts the results of an investigation from 1500 nm to 1600 nm of an example, the TE0–TE1 mode multiplexer, that show the possible errors of the waveguide separation D , access waveguide width W_a , and bus waveguide width W_b . The conversion efficiency remained greater than -0.7 dB and the crosstalk remained less than -35 dB for waveguide separation variations as large as $\pm 40 \text{ nm}$, access-waveguide width variations of $\pm 10 \text{ nm}$, and bus-waveguide width variations as large as $\pm 20 \text{ nm}$. The fabrication tolerance for the access-waveguide width variations is approximately $\pm 10 \text{ nm}$, which can be further improved by varying the width of the multimode bus waveguide along the device (which is fixed in our work), or by using other protocol of STA.

According to the accurate analysis and experimental results of ADC based mode (de)multiplexers [4,7], the coupling length of TE0–TE1 (de)multiplexer is 13.773 μm (100 nm gap) or 31.732 μm (200 nm gap), the crosstalk is below -23 dB , and insertion loss is $<1 \text{ dB}$ over a 20-nm bandwidth. For the adiabatic coupler based TE0–TE1 (de)multiplexer [11], the coupling length is 200 μm , the crosstalk is $<-13 \text{ dB}$, and insertion loss is $<1 \text{ dB}$ over a 180-nm bandwidth. For our STA-based TE0–TE1 (de)multiplexer, the coupling length is 100 μm , the crosstalk is $<-24 \text{ dB}$, and insertion loss is $<1.3 \text{ dB}$ over a 100-nm bandwidth. So our (de)multiplexers have broader bandwidth compared with the ADC based devices and have smaller device sizes and lower crosstalk compared with other adiabatic coupler based devices.

4. Conclusion

We have presented experimental demonstration of a series of broadband, low-loss, and low-crosstalk mode (de)multiplexers based on an SOI platform using the protocol of STA for the first time. All five two-mode MDM links demonstrated measured insertion losses less than 1.1 dB. Associated crosstalks were lower than -24 dB over a broad wavelength range from 1500 nm to 1600 nm. The four-mode MDM link showed measured insertion losses less than

1.3 dB. In this case, the crosstalks were lower than -23 dB within the same wavelength range. Thus, these MDM links can be integrated with other multiplexing technologies to increase transmission capabilities. Moreover, a similar method can be used to design and fabricate other passive devices like power splitters and polarization controllers.

Funding

National Natural Science Foundation of China (NSFC) (61575189, 61635011).